Rapid Flow-Through Biocatalysis with High Surface Area, Enzyme-Loaded Carbon and Gold-Bearing Diatom Frustule Replicas

Stan C. Davis, Vonda C. Sheppard , Gousia Begum, Ye Cai, Yunnan Fang, John D. Berrigan, Nils Kröger, and Kenneth H. Sandhage**

Hierarchically-porous, rigid inorganic structures have attracted appreciable interest in a wide range of applications, including catalysis, filtration, sensing, and energy storage/harvesting. Naturally-occurring, hierarchically-porous, rigid assemblies with a wide range of three-dimensional (3D) structures are generated by diatoms (photosynthetic aquatic microorganisms); that is, each of the tens of thousands of diatom species forms a macro-to-mesoporous, silica-bearing cell wall (frustule) with a particular, highly-reproducible 3D morphology. We have recently demonstrated that such intricate biosilica structures can be converted, without loss of 3D morphology, into high surface area (>1300 m^2/g) macro-to-microporous carbon. Here we demonstrate, for the first time, how the chemical tailoring of such hierarchically-porous, carbon-converted, 3D biogenic structures can result in a high degree of enzyme loading for rapid flow-through catalysis. Two approaches have been developed for enriching such structures with carboxylic acid groups: i) dendritic amplification of partially-oxidized C replicas, and ii) electrochemical Au deposition followed by self-assembly of a carboxylic acid-bearing surface layer. The terminal carboxylic acid groups were then used for electrostatic attachment of a protamine (PA) modified derivative of the model enzyme, glucose oxidase (GOx-PA). In a flow-through system, the GOx-PA-loaded, diatom-derived microscale structures displayed a glucose consumption rate more than 80% faster than for GOx-PA-loaded C black and Au nanoparticles. The rapid flow-through catalysis of the carbon and gold-bearing frustule replicas was enabled by the open 3D morphology of the starting diatom silica templates, along with the enhanced surface area and high enzyme loading resulting from the chemical conversion and surface functionalization processes.

1. Introduction

Functional enzymes immobilized on solid supports are utilized in a wide range of applications, including environmental sensing,[1a] medical diagnostics,[1b] organic syntheses,[1c,d] and energy harvesting.[1e–h] Porous, high surface area materials are particularly desired as enzyme supports for providing high binding capacities for the enzymes and, in some cases, protecting enzyme molecules located inside the pores from thermal denaturation (e.g., from temperature fluctuations) or (bio)chemical degradation (e.g., by microbes).[2] Commonly-used porous support materials for enzyme immobilization include silica,[2a,2b,3] carbon,[1e–h,4] gold,[5] and combinations of these materials.[6]

Hierarchically-porous materials can be particularly advantageous as enzyme supports in flow-through reactors, with large macropores (>50 nm diameter) enabling rapid fluid transport and smaller mesopores (2–50 nm diameter) providing a high specific surface area for enzyme loading.[7] A wide variety of naturally-occurring, hierarchically-patterned, three-dimensional (3D) structures are generated by diatoms (single-celled, photosynthetic aquatic algae). Each of the tens of thousands of diatom species forms a

Dr. S. C. Davis, Dr. Y. Cai, Dr. Y. Fang, Dr. J. D. Berrigan, Prof. N. Kröger, Prof. K. H. Sandhage
School of Materials Science and Engineering
Georgia Institute of Technology
Atlanta, GA 30332, USA
E-mail: kroeger@bcube-dresden.de; ken.sandhage@mse.gatech.edu
Dr. V. Sheppard
Metrics, Inc
Greenville, NC 27834, USA

Dr. V. Sheppard, Dr. G. Begum, Prof. N. Kröger, Prof. K. H. Sandhage
School of Chemistry and Biochemistry
Georgia Institute of Technology
Atlanta, GA 30332, USA
Dr. J. D. Berrigan
Soft Matter Materials Branch (RXAS)
Air Force Research Laboratory
Wright-Patterson Air Force Base, OH 45433, USA
Prof. N. Kröger
ZIK B CUBE and Department of Chemistry and Food Chemistry
Dresden Institute of Technology (TU Dresden)
01307 Dresden, Germany

DOI: 10.1002/adfm.201203758

macro-to-mesoporous silica microshell (frustule) with a particular (species-specific) 3D morphology.[8] Diatom frustules are abundant and readily available at low cost as diatomaceous earth. While the hollow, macroporous nature of diatomaceous earth could yield powder compacts exhibiting low pressure drops in a flow-through reactor, the typical values of specific surface area and specific mesopore volume of diatomaceous earth ($\leq 10^1$ m^2 g^{-1} and ≤ 0.01 cm^3 g^{-1}, respectively) are rather modest for use in enzyme adsorption. In addition, the poor electrical conductivity of diatom silica inhibits the use of this material for electrode applications (e.g., in biofuel cells or amperometric sensors).

The inorganic chemistry and properties of diatom silica may be altered over a wide range, without loss of the hollow, 3D frustule morphology through the use of gas/solid displacement reactions,[9] conformal coatings,[10] or both.[11] Recent work by some of the co-authors has shown that diatomaceous earth may be converted into high surface area (>1300 m^2 g^{-1}) carbon replicas with high specific mesopore and micropore volumes.[9g] Here we explore, for the first time, the utility of such highly-porous, hollow carbon microparticles as enzyme supports for flow-through catalysis. Electrochemical conversion of the carbon frustule replicas into porous gold-bearing replicas is also examined. Approaches for functionalizing such open, hierarchically-porous carbon and gold-bearing microparticles are evaluated to allow for a high degree of loading of the model enzyme, glucose oxidase (GOx). The rates of glucose consumption through powder beds of these enzyme-bearing, frustule-shaped carbon and gold-bearing microparticles are then compared to enzyme-bearing commercially-available carbon black and gold nanoparticles via use of an in-line, flow-through system.

2. Results and Discussion

2.1. Functionalization of High Surface Area Carbon Replicas of Diatom Frustules

A secondary electron (SE) image of a starting silica-based frustule of the diatom *Aulacoseira* (obtained as diatomaceous earth) is shown in **Figure 1** a. These frustules possessed a hollow,

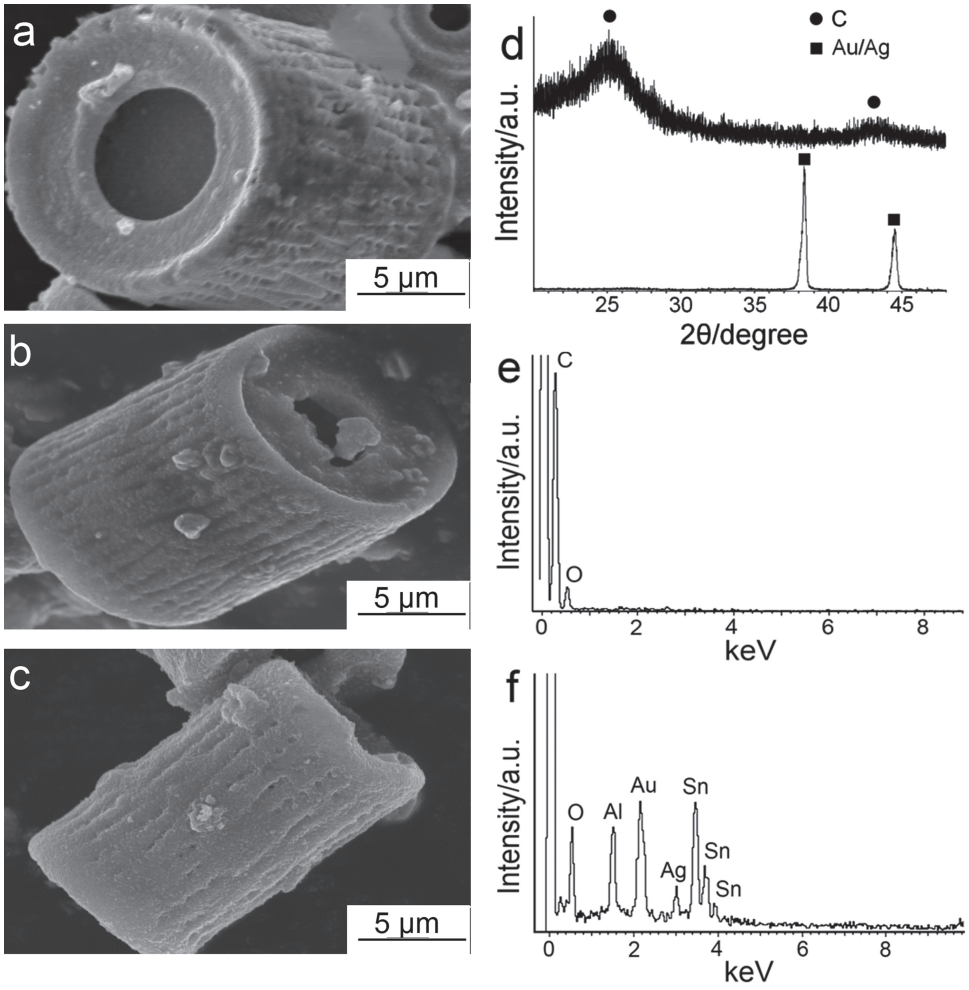

Figure 1. Structural analyses of diatom silica and diatom-derived carbon and gold-bearing replicas. SE images of: a) an *Aulacoseira* silica diatom frustule obtained as diatomaceous earth ($dSiO_2$), b) a carbon frustule replica after a 48 h treatment with HNO_3 (dC_{Ox}), and c) a gold-bearing frustule replica (dAAS). d) Glancing angle XRD analyses of dC_{Ox} and dAAS specimens. e) EDX analysis of a dC_{Ox} specimen. f) EDX analysis of a dAAS specimen (note: the Al peak was associated with the specimen support).

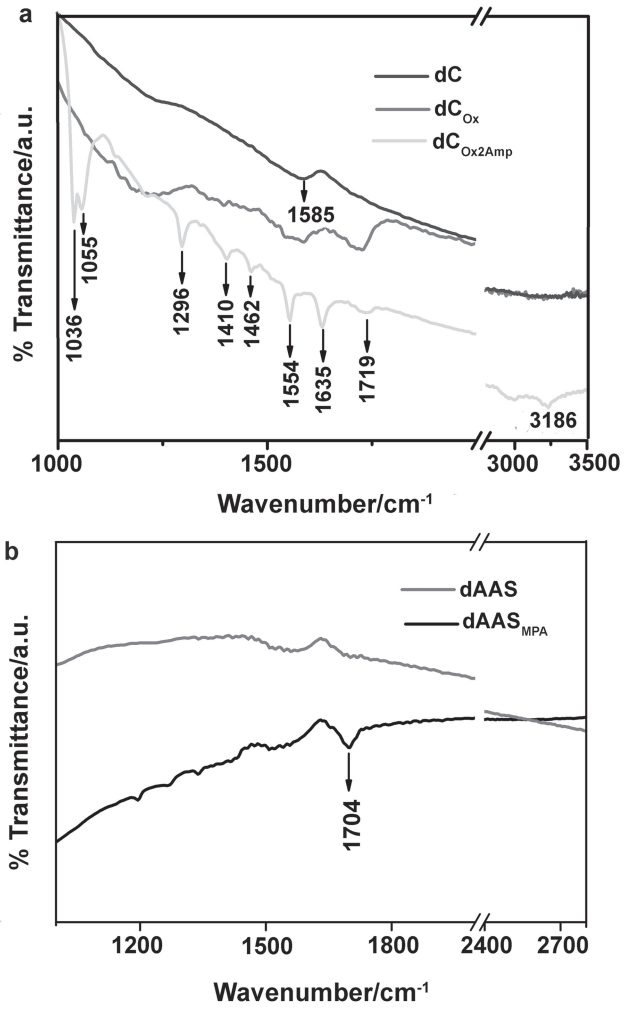

Figure 2. FTIR analyses of diatom frustule replicas. a) Spectra obtained from dC, dC_{Ox}, and dC_{Ox2Amp} specimens. b) Spectra obtained from dAAS and $dAAS_{MPA}$ specimens.

cylindrical geometry with open ends containing a protruding rim and with rows of fine pores running parallel to the long frustule axis. A series of gas/solid reactions was used to convert these silica frustules into highly-porous carbon replicas, according to a previously-published method.[9g] In short, the silica was first converted, via magnesiothermic reduction at 900 °C, into an interpenetrating two-phase composite of magnesia and silicon.[9a,c] After selective magnesia dissolution, the resulting porous silicon replicas[9f] were exposed to methane at 950 °C and then thermally treated at a peak temperature of 1200 °C to allow for conversion into silicon carbide. Finally, the silicon was selectively removed from silicon carbide, via selective reaction with chlorine at 950 °C, to yield carbon replicas (as confirmed by XRD and EDX analyses of the types shown in Figures 1d and e, respectively).[9g] Fourier transform infrared (FTIR) analysis (**Figure 2**a) of the carbon-converted frustules (referred to herein as dC specimens) revealed an absorption band at 1585 cm^{-1}, which was consistent with C=C stretching vibrations associated with sp^2-hybridized amorphous carbon.[12a,b] As shown in **Table 1**, the carbon-converted frustules possessed values of specific surface area (SSA) and specific mesopore volume, for 2–50 nm diameter pores (SMeV(2–50)) and for 22–50 nm diameter pores (SMeV(22–50)), that were more than two orders of magnitude higher than for the starting silica frustules ($dSiO_2$ specimens). Furthermore, unlike the $dSiO_2$ specimens, the dC specimens possessed appreciable microporosity (Supporting Information Table S1 and Figure S1). To allow for comparisons of enzyme loading and catalytic activity relative to these carbon frustule replicas, Vulcan XC-72R carbon black microparticles (4.9 μm average diameter) were also utilized in this work (VC specimens).

To enable electrostatic binding of enzymes with net positive charges (see below), the introduction of negative charges to carbon frustule replicas was examined via oxidation in an aqueous 2.6 M nitric acid solution at 75 °C for varied times.[13] An increase in the nitric acid exposure time from 1 to 48 h resulted in a monotonic increase in the magnitude of the negative zeta potential of the carbon replica microparticles at pH 7.0 (Supporting Information Table S2). FTIR analyses (Figure 2a)

Table 1. Specific values of surface area, mesopore volume, enzyme loading, and catalytic activities of diatom silica, diatom-derived replicas, and reference particles. The amount of GOx-PA enzyme bound to the supports was determined via enzyme activity. One unit (1 U) of GOx-PA activity corresponded to 1 μmol glucose consumed per minute. SSA: specific surface area, SMeV(2–50): specific mesopore volume for pores 2–50 nm in diameter, SMeV(22–50): specific mesopore volume for pores 22–50 nm in diameter, n.d.: not determined, and b.d.l.: below detection limit.

Sample	SSA [m^2g^{-1}]	SMeV(2–50) [cm^3g^{-1}]	SMeV(22–50) [cm^3g^{-1}]	Enzyme Loading [10^{-3} g enzyme g^{-1} support]	Specific Activity [10^{-3} Ug^{-1} GOx-PA]
$dSiO_2$	1.72	0.005	5.91×10^{-4}	1.9	56.0
dC	1330	1.530	0.120	n.d.	n.d
dC_{Ox}	793	1.160	0.0835	34.6	n.d
dC_{Ox1Amp}	180	0.307	0.0189	63.7	51.3
dC_{Ox2Amp}	93.8	0.084	6.05×10^{-3}	55.5	n.d
VC	227	0.413	0.101	n.d	n.d
VC_{Ox}	63.6	0.037	2.29×10^{-3}	12.3	25.3
dAAS	127	0.206	7.97×10^{-3}	0.7	n.d
$dAAS_{MPA}$	64.2	0.052	1.90×10^{-3}	15.7	49.3
$AuNP_{MPA}$	1.17	b.d.l.	1.20×10^{-5}	10.1	20.7

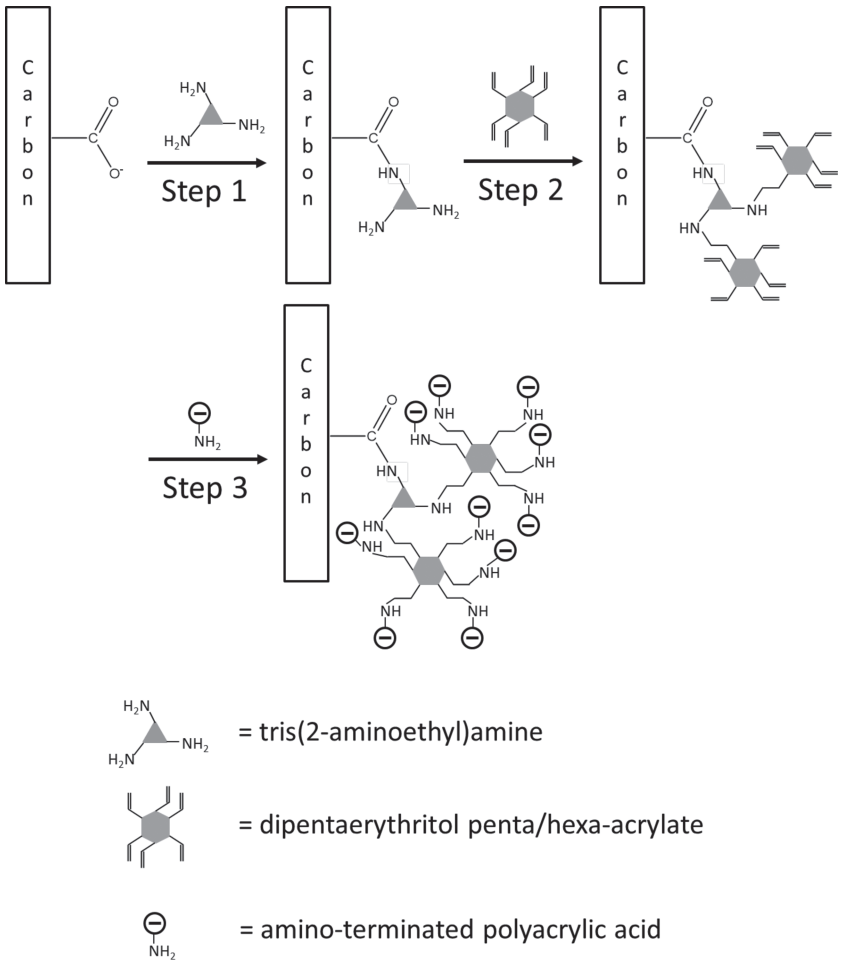

Scheme 1. Illustration of the reaction sequence used for the dendritic amplification of carboxylic acid groups on the surfaces of dC_{Ox} microparticles.

revealed the absence and presence of the C=O stretching vibration (at 1719 cm^{-1}) before and after the 48 h nitric acid treatment, respectively, which was consistent with oxidation-induced generation of surface carboxylate anions. After the 48 h nitric acid treatment, the carbon frustule replicas (dC_{Ox} specimens) retained the *Aulacoseira* frustule morphology (Figure 1b), whereas nitric acid exposure for 72 h resulted in oxidative disintegration of the frustule structure (Supporting Information Figure S2). Hence, for subsequent experiments, nitric acid treatments were limited to 48 h. To introduce carboxylate groups onto the VC specimens, nitric acid treatment was also limited to 48 h (VC_{Ox} specimens).

To further increase the surface density of carboxylate anions, while avoiding oxidative destruction of the frustule 3D morphology, the binding of additional carboxylate groups to the dC_{Ox} microparticles was examined via the dendritic amplification protocol illustrated in **Scheme 1**.[14] The carboxylate groups on the dC_{Ox} microparticles were activated for reaction with amines through exposure to a buffered (pH 5.9) solution of 1-ethyl-3-(3Dimethylaminopropyl) carbodiimide (EDC) and sulfo-N-hydroxysuccinimide (SNHS).[14a] The microparticles were then allowed to react with a polyamine, tris(2-aminoethyl)amine (TAEA), to generate two primary amines at the site of each reacted surface carboxyl group (Scheme 1, step 1). These primary amines were then allowed to undergo a Michael addition reaction with a polyacrylate monomer, dipentaerythritol penta/hexa-acrylate, so as to generate up to 5 pendant acrylate groups per reacted primary amine (Scheme 1, step 2). The available acrylate groups were then exposed to an amino-terminated polyacrylic acid to introduce, via Michael addition, up to 32 new carboxyl groups for each reacted acrylate group (Scheme 1, step 3). The zeta potential value of HNO_3-treated carbon frustule replicas that underwent this amplification treatment (dC_{Ox1Amp} specimens) was more negative than for the dC_{Ox} specimens (−31.1 mV vs. −23.0 mV at pH 7.0), which was consistent with increased loading of carboxylate anions by the amplification treatment. In an attempt to obtain an even higher density of surface carboxylate groups, dC_{Ox} microparticles were subjected twice to the dendritic amplification steps 1 and 2 (Scheme 1), followed by step 3 (dC_{Ox2Amp} specimens). FTIR analyses (Figure 2a) of dC_{Ox2Amp} specimens revealed an absorption band at 1719 cm^{-1}, which was consistent with the C=O stretching vibration of carboxylic acids. Additional absorption bands in the FTIR spectrum demonstrated the presence of functional groups associated with the reacted polyamines and polyacrylates used in the amplification process (see also Supporting Information Figure S4a and Table S3).[12a,b]

In order to determine the effects of the nitric acid and dendritic amplification treatments on the surface area and mesopore volumes of the carbon frustule replicas, nitrogen adsorption analyses were conducted after each step (Table 1, Supporting Information Table S1). The 48 h HNO_3 treatment (dC_{Ox} specimens) led to significant decreases in SSA, SMeV(2–50), SMeV(22–50), and SMiV relative to the dC specimens. The enrichment of carboxylate groups on the dC_{Ox} specimens after a single amplification cycle (dC_{Ox1Amp} specimens) resulted in further decreases in SSA, SMeV(2–50), and SMeV(22–50) (Table 1). Additional reductions in SSA, SMeV(2–50), and SMeV(22–50) were observed with the binding of carboxyl groups via two dendritic amplification cycles (dC_{Ox2Amp} specimens). Nonetheless, the dC_{Ox1Amp} and dC_{Ox2Amp} specimens still possessed appreciably larger values of SSA, SMeV(2–50), and SMeV(22–50) (by 47–180%, 130–730%, and 160–730%, respectively) than the VC_{Ox} specimens.

2.2. High Surface Area, Functionalized Gold-Bearing Replicas of Diatom Frustules

Gold has also been utilized by several authors as a conductive template for enzyme immobilization.[5] While the conversion

of silica diatom microshells into freestanding gold-bearing replicas has been previously reported by a few authors, the specific surface areas of such frustule-shaped microparticles were modest (e.g., ≤10.1 m^2 g^{-1}).[15] To investigate whether gold-bearing frustule replicas with much higher SSA values could be synthesized, an electrochemical deposition/reaction process was examined for converting the high SSA carbon frustule replicas into gold.

dC_{Ox} specimens were sensitized for electroless deposition via exposure to an acidic solution of tin(II) chloride.[16] The specimens were then exposed to a basic solution of silver nitrate for 15 min to allow for electroless silver deposition. After washing, the specimens were pyrolyzed in air at 300 °C to remove the underlying carbon template, which was confirmed by thermogravimetric analysis (Supporting Information Figure S3). The silver-bearing frustule replicas were then exposed to an aqueous solution of chloroauric acid at 100 °C for 10 min to allow for the deposition of gold via the following displacement reaction[17]:

$$3Ag(s) + HAuCl_4(aq) => Au(s) + 3AgCl(aq) + HCl(aq) \quad (1)$$

X-ray fluorescence (XRF) analysis indicated that the resulting replicas were comprised of 37.9 wt% gold, 14.1 wt% silver, and 48.0 wt% tin (metals basis), which corresponded to 16.3 vol% gold, 11.0 vol% silver, and 72.7 vol% tin oxide (SnO_2).[18] Energy dispersive X-ray (EDX) analysis of these frustule replicas also revealed the presence of substantial amounts of tin and oxygen, along with gold and silver (Figure 1f). SE images revealed that the morphologies of these frustule replicas (dAAS specimens, where AAS refers to Au, Ag, and SnO_2) were similar to that of the starting silica frustules (Figures 1a and c). Exposure of the silver-bearing specimens to the chloroauric acid solution for a longer time of 30 min, to allow for more complete replacement of the silver with gold, resulted in the formation of appreciable gaps in the frustule structure. (Note: the exchange of three silver atoms for one gold atom by reaction (1) results in 67% loss in solid volume.)[18] X-ray diffraction (XRD) analysis of the dAAS microparticles (Figure 1d) revealed only diffraction peaks consistent with Au and Ag. Scherrer analysis of these diffraction peaks yielded an average crystal size of 35 nm.

A bright field transmission electron (TE) image of an ion-milled cross-section of a dAAS specimen is shown in **Figure 3**a. The former frustule wall was comprised of fine particles (≈30–150 nm diameter) dispersed in a matrix phase, with a higher concentration of such particles located at the outer surface. Selected area electron diffraction (SAED) analysis (Figure 3b) revealed the presence of Au and/or Ag along with crystalline SnO_2. EDX analyses (Supporting Information Figure S5) indicated that the particles were rich in gold and silver, whereas the matrix phase was rich in tin and oxygen. High resolution TE analysis (Figure 3c) revealed lattice fringes for the fine particles with spacings consistent with Ag or Au, and lattice fringes for crystals in the matrix with spacings consistent with SnO_2. Although some crystalline tin oxide was detected by SAED analysis, the absence of detectable diffraction peaks by XRD analysis (Figure 1d) indicated that the matrix was largely comprised of amorphous tin oxide. Nitrogen adsorption analysis (Table 1) indicated that the dAAS

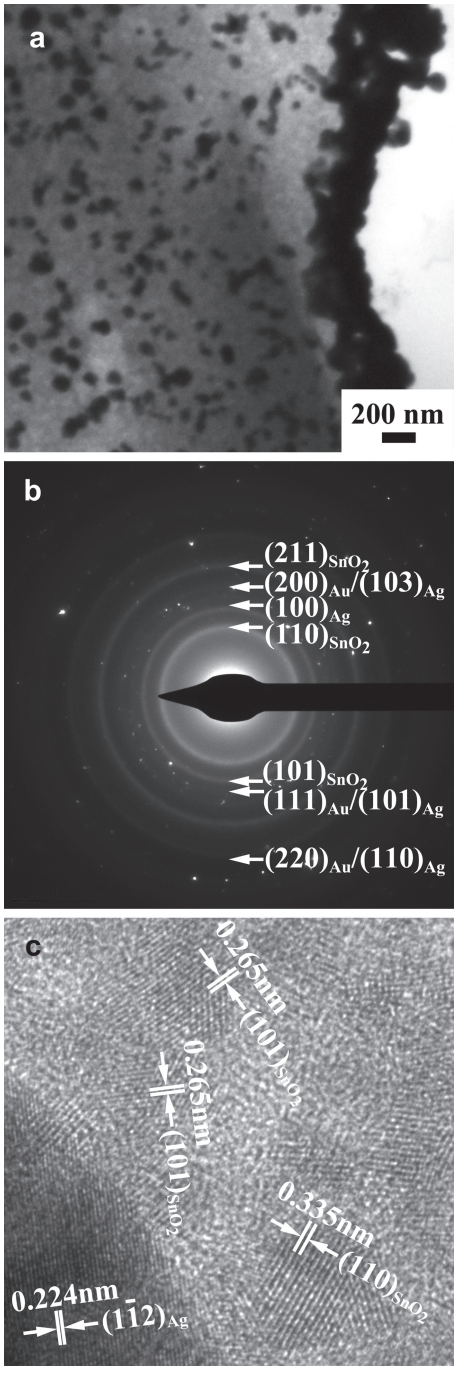

Figure 3. TE analysis of an ion-milled cross-section of a dAAS specimen. a) Bright-field TE image. b) SAED analysis. c) High resolution TE image.

specimens possessed a SSA of 127 m^2 g^{-1}, which was an order of magnitude higher than has previously been reported for gold-bearing frustule replicas.[15a]

To enable enzyme loading via electrostatic interactions, the surfaces of the dAAS specimens were exposed to an ethanolic solution of 3-mercaptopropionic acid (MPA), to allow for the formation of a self-assembled MPA layer displaying pendant carboxylic acid groups.[19] The absence of a characteristic S-H

stretching absorption band (at 2573 cm^{-1}) and the presence of a C=O stretching absorption (at 1704 cm^{-1}) in the FTIR analysis (Figure 2b and Supporting Information Figure S4b) were consistent with the formation of gold-thiolate bonds and the presence of carboxylic acid groups, respectively, on the MPA-treated gold-bearing frustule replicas ($dAAS_{MPA}$ specimens).[12c] The presence of the MPA layer on the $dAAS_{MPA}$ specimens resulted in reductions in the SSA, SMeV(2–50), and SMeV(22–50) values relative to the dAAS specimens (Table 1). To enable comparisons of enzyme loading and catalytic activity relative to these gold-bearing frustules-shaped templates, commercial gold nanoparticles (AuNP specimens, 50–100 nm diameter) were also functionalized with MPA ($AuNP_{MPA}$ specimens) using the same method as for the gold-bearing frustule replicas.

2.3. Enzyme Immobilization on Functionalized Carbon and Gold-Bearing Diatom Frustule Replicas

Glucose oxidase (GOx), a 128 kDa homodimer from the fungus *Aspergillus niger*, was chosen as a model enzyme to evaluate the efficacy of $dSiO_2$, dC_{Ox1Amp}, VC_{Ox}, $dAAS_{MPA}$, and $AuNP_{MPA}$ specimens as supports for enzyme immobilization. GOx possesses a highly negative net charge at neutral pH (isoelectric point = 4.2)[20] and, thus, should be electrostatically repelled from the negatively-charged surfaces of the above specimens. Indeed, only small amounts of GOx were found to bind to these specimens (Supporting Information Table S1). It has previously been shown that GOx adopts a positive charge at neutral pH after chemical cross-linking with protamine (PA),[21] a natural polycationic peptide harvested from fish sperm (primary sequence: $^{+}H_3N$-ARRRRSSSRPIRRRRPRRRTTRRRRA-GRRRR-CO_2^-). The resulting GOx-PA molecule possesses a hydrodynamic diameter of 22.4 ± 3.7 nm and exhibits the same specific activity as GOx.[21] One to two orders of magnitude greater amounts of GOx-PA than GOx could be loaded onto $dSiO_2$, dC_{Ox1Amp}, VC_{Ox}, $dAAS_{MPA}$, and $AuNP_{MPA}$ specimens (Table 1; Supporting Information Table S1 and Figure S6) which demonstrated the efficacy of the PA moiety for promoting enzyme binding to carboxylated surfaces. The specific values of GOx-PA loading capacity for the silica frustules and oxidized carbon specimens followed similar trends as for the values of SSA and SMeV(22–50) (i.e., for pores in the 22–50 nm range that GOx-PA could access); that is, these values increased in the order $dSiO_2 < VC_{Ox} < dC_{Ox1Amp}$.

The dC_{Ox1Amp} microparticles exhibited the highest specific enzyme loading capacity for GOx-PA (Table 1), although this specimen possessed substantially lower values of SSA and SMeV(22–50) compared to the dC_{Ox} specimens. This discrepancy could be explained by the higher apparent density of negative charges on the surfaces of the dC_{Ox1Amp} specimens (ζ = –31.1 mV) relative to the surfaces of dC_{Ox} microparticles (ζ = –23.0 mV); that is, the decrease in SSA and SMeV(22–50) resulting from the filling of mesopores by the dendritic amplification process was offset by the increase in density of negative charges available for electrostatic binding to the positively-charged GOx-PA molecules. The specific loading capacity for GOx-PA detected for dC_{Ox2Amp} specimens was noticeably lower than for dC_{Ox1Amp} specimens, which was consistent with further decreases in SSA and SMeV(22–50) resulting from increased filling of pores with organic moieties upon repetition of the first two steps of the dendritic amplification process. The specific loading capacities for GOx-PA were substantially higher for dC_{Ox} and dC_{Ox1Amp} specimens than for VC_{Ox} specimens (by 180% and 420%, respectively) and for $dAAS_{MPA}$ specimens than for $AuNP_{MPA}$ specimens (by 55%), which was consistent with the enhanced and readily-accessible surface areas resulting from the hollow nature and relatively high mesopore volumes of the diatom-derived replicas.

2.4. Flow-Through Catalysis by Immobilized GOx-PA

To compare catalytic performances in a "flow-through" system, each type of GOx-PA-bearing template was incorporated as a powder bed (0.2 mL) into an inline filtration apparatus (**Scheme 2**). A circulating stream of substrate solution was then pumped through the powder bed at a constant rate (10 mL min^{-1}). Small aliquots of the substrate solution were withdrawn periodically to evaluate the remaining glucose content as a function of time. A steady decline in the glucose concentration was observed as a function of time (**Figure 4**a) for all support materials ($dSiO_2$, dC_{Ox1Amp}, VC_{Ox}, $dAAS_{MPA}$, and $AuNP_{MPA}$) containing immobilized GOx-PA. No glucose loss was detected from the substrate solution when the same support materials were tested without the attached enzyme. Within the first 15 min, an approximately constant rate of decline in glucose concentration was observed for each sample tested (Figure 4b). This initial rate of glucose consumption was highest for GOx-PA immobilized on dC_{Ox1Amp} and $dAAS_{MPA}$ microparticles, and lowest for GOx-PA immobilized on $AuNP_{MPA}$ and $dSiO_2$ microparticles, while VC_{Ox} specimens exhibited an intermediate glucose consumption rate (Figure 4b). This trend was largely consistent with the

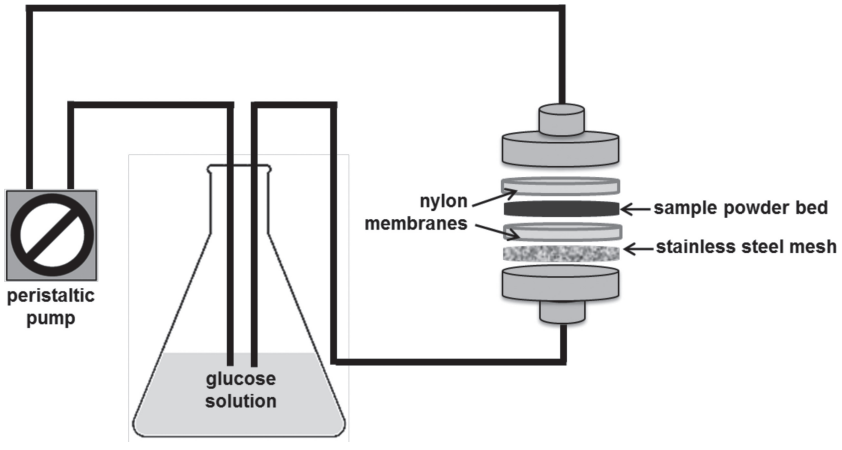

Scheme 2. Schematic illustration of the in-line (flow-through) filtration system used for testing the rate of glucose consumption catalyzed by GOx-PA-loaded microparticles.

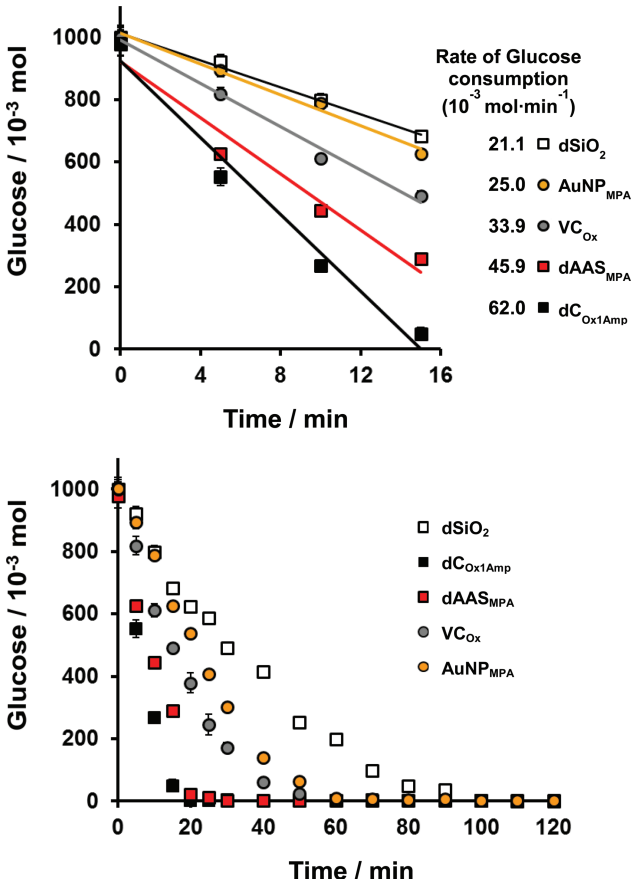

Figure 4. Glucose consumption as a function of time during flow-through catalysis with GOx-PA-bearing supports. GOx-PA was immobilized on diatom silica ($dSiO_2$), frustule-derived microparticles (dC_{Ox1Amp}, $dAAS_{MPA}$), and reference particles ($AuNP_{MPA}$, VC_{Ox}). Each data point represents the average of six measurements. The data plotted in (b) were obtained for only the first 15 min of flow-through catalysis shown in a), and the associated rate constants for each type of support are presented in (b) for this apparent linear regime of glucose consumption.

differences in the specific enzyme capacity of the specimens (Table 1). The only exception was for $dSiO_2$ specimens, which exhibited almost the same initial glucose consumption rate as for $AuNP_{MPA}$ specimens despite a 5.3-fold lower value of specific enzyme loading capacity.

To assess the catalytic performance of the various enzyme-bearing specimens independent of their specific enzyme capacity, the initial glucose consumption rates were normalized to the amounts of immobilized GOx-PA (Table 1). This yielded specific catalytic activities which were direct measurements of the average catalytic efficacy of GOx-PA molecules immobilized on a given solid support. Remarkably, the three samples with diatom-derived microparticle morphologies ($dSiO_2$, dC_{Ox1Amp}, and $dAAS_{MPA}$) exhibited similar specific catalytic activities ($49.3–56.0 \times 10^{-3}$ Ug^{-1}) that were 95–170% higher than the specific catalytic activities of the enzyme-loaded specimens derived from commercially-available support materials ($20.7–25.3 \times 10^{-3}$ Ug^{-1}). This result indicated that diatom silica and the diatom-derived replicas strongly promoted the interaction of the immobilized enzyme, GOx-PA, with the substrate, glucose, relative to conventional enzyme support materials.

3. Conclusions

The present work demonstrates the attractive properties of diatom-derived carbon and gold-bearing replica microparticles as support materials for enzyme immobilization. Upon shape-preserving inorganic conversion and appropriate surface functionalization (to allow for relatively high enzyme loading), the flow-through catalytic activities of the GOx-PA-bound carbon and gold-bearing frustule replicas were noticeably enhanced relative to the starting silica frustules and to conventional enzyme support materials. Furthermore, after normalization with respect to the amount of enzyme loading, the specific enzyme activities of all of the GOx-PA-bearing frustule-shaped supports (diatom silica, diatom-derived carbon and gold-bearing replicas) were similar and reproducibly higher than for conventional enzyme supports that lacked the frustule morphology.

To our knowledge, this is the first demonstration of the coupling of the architecture of a 3D bio-inorganic template with shape-preserving inorganic conversion and surface molecular tailoring to enhance the flow-through catalytic activity of an immobilized enzyme. The silica transformation and surface functionalization approaches developed in this work may be applied to a variety of synthetic or other biogenic silica templates. Indeed, the wide variety of hierarchical pore structures available in diatom frustules and other bio-silica templates provide a rich palette of morphologies to interrogate for use of such chemical modification for further enhancements of enzyme loading and specific flow-through catalytic activity. This general chemical modification and molecular tailoring strategy may also be used to immobilize other functional enzymes for energy harvesting, fluid purification, sensing, (bio)chemical syntheses, or other applications.

4. Experimental Section

Chemicals: Milli-Q purified water (resistivity 18.2 MΩ cm) was used for all solutions and washing steps. 1-Ethyl-3-(3-dimethylaminopropyl)carbodiimide (EDC), sodium hydroxide, tris(hydroxymethyl)aminomethane, and tin(II) chloride were purchased from Alfa Aesar (Ward Hill, MA). Glucose oxidase (100 U/mg solid) from *Aspergillus niger*, protamine sulfate from salmon sperm, 3-mercaptopropionic acid (MPA), potassium bromide, sulfo-N-hydroxysuccinimide (SNHS), 2-mercaptoethanol, tris(2-aminoethyl)amine (TAEA), dipentaerythritol penta/hexa-acrylate, and $HAuCl_4$ were purchased from Aldrich (St. Louis, MO). Nitric acid, methanol, ethanol, and hydrochloric acid were purchased from VWR (West Chester, PA). Dibasic and monobasic sodium phosphate were purchased from Amresco (Solon, OH). 2-(N-morpholino)ethanesulfonic acid (MES) was purchased from J.T. Baker (Phillipsburg, NJ). Trifluoroacetic acid was purchased from American Bioanalytical (Natick, MA). Silver nitrate was purchased from Mallinckrodt (Paris, KY). Ammonium hydroxide was purchased from Fisher Scientific (Fair Lawn, NJ). Amino-terminated polyacrylic acid (P5839A-AANH2) was purchased from Polymer Source, Inc. (Montreal, Quebec). Bis[sulfosuccinimidyl] suberate (BS^3) was purchased from Thermo Scientific (Rockford, IL)

Surface Modification of Carbon Diatom Frustule Replicas: Carbon diatom replicas (dC) were fabricated using a previously-reported method.[9g] To introduce surface carboxyl groups, the carbon-converted replicas (100 mg) were suspended in an aqueous HNO_3 solution (250 mL, 2.6 M) and refluxed at 75 °C for 1–48 h. After this treatment, the carbon replicas were washed by 5 min of centrifugation (4260 *g*) with deionized water (three times), and then methanol (twice), followed by drying overnight at 60 °C.

To amplify surface carboxyl groups on carbon frustule replicas that had been exposed to the nitric acid treatment for 48 h (dC_{Ox} specimens), the dried replicas (5 mg) were suspended in an aqueous solution of MES-NaOH buffer (5 mL, 100 mM, pH 5.85) with EDC (4 mg) and SNHS (12 mg) for 2 h. At the end of the treatment, 3-mercaptoethanol (14 µL) was introduced into the suspension which was then stirred for 10 min. The solid material was washed by 5 min of centrifugation (4260 *g*) in deionized water (three times), and then in a PBS buffer solution (4 mL, 100 mM NaH_2PO_4, 100 mM Na_2HPO_4, 150 mM NaCl, pH 7.2). After adding TAEA (1 mL), the suspension was stirred for 2 h, and then washed by 5 min of centrifugation (4260 *g*) in deionized water (three times), and then methanol (twice), followed by drying overnight at 60 °C. The dried powder was then suspended in a solution comprised of ethanol (8 mL) and dipentaerythritol penta//hexa-acrylate (4 mL) for 2 h at room temperature. After washing by 5 min of centrifugation (4260 *g*) in ethanol (three times), the solid material was suspended in a solution of amino-terminated polyacrylic acid (8 mg) in ethanol (5 mL) for 2 h at room temperature (yielding dC_{Ox1Amp}). The dC_{Ox1Amp} particles were washed by 5 min of centrifugation (4260 *g*) in ethanol (three times) followed by drying overnight at 60 °C.

Synthesis of High Surface Area Gold-Bearing Diatom Replicas: The dC_{Ox} specimens were incubated for 1 h at room temperature in a solution of $SnCl_2$ (26 mM) and trifluoroacetic acid (70 mM) in H_2O/MeOH (1:1). The samples were then washed by 5 min of centrifugation (4260 *g*) in deionized water (three times), then in methanol (twice), followed by drying overnight at 60 °C. The Sn(II)-loaded dC_{Ox} powder was suspended in an aqueous solution of $AgNO_3$ (30 mM) that had been titrated with NH_4OH (0.01 M) until the solution became colorless, and incubated for 15 min at room temperature. The resulting material was washed by 5 min of centrifugation (4260 *g*) with water (three times) and then methanol (twice). The carbon was then removed from the specimens by pyrolysis at 300 °C in air. The resulting material (10 mg) was then exposed at 100 °C to an aqueous solution (50 mL) of $HAuCl_4$ (10 µmol) to yield gold-bearing frustule replicas (dAAS specimens). The dAAS specimens were washed by 5 min of centrifugation (4260 *g*) in deionized water (three times), then in methanol (twice), followed by drying overnight at 60 °C.

Coating of dAAS and AuNP with MPA: dAAS or AuNP particles (10 mg) were suspended in a solution of MPA (1 M) in ethanol, and then stirred for 24 h at room temperature, to yield $dAAS_{MPA}$ or $AuNP_{MPA}$ specimens. These specimens were washed by 5 min of centrifugation (4260 *g*) in deionized water (three times), then in methanol (twice), followed by drying overnight at 60 °C.

Immobilization of GOx-PA: A given support material (1 mg of diatom silica, diatom-derived replicas, or reference materials) was suspended in an aqueous solution of Tris-HCl (50 mM, pH 7.0) containing varied amounts (up to 100 µg) of GOx-PA (synthesized as previously described)[21] at room temperature for 20 h with stirring. The mixture was centrifuged for 5 min at 16 000 *g* and the supernatant was retained. The pellet was washed three times with a 50 mM Tris-HCl buffer (pH 7.0) solution and then resuspended in the same buffer (0.25 mL). The amount of GOx-PA present in the suspension (immobilized GOx-PA), as well in the supernatant (unbound GOx-PA), was determined through an activity assay as described previously.[21] Repeated measurements for the same type of template indicated less than 5% variation in the amount of detected GOx-PA loading. The specific activity of GOx-PA was not affected by binding to any of the substrates used in this study. This was demonstrated by the observation that, for each type of support specimen, the combined value of the measured activities of bound and unbound (remaining in solution) GOx-PA equaled the measured activity of the completely unbound enzyme (i.e., the combined, bound plus unbound, value corresponded to a relative activity of 100%), as shown in Supporting Information Figure S6. For the $dAAS_{MPA}$ specimens, SnO_2 had little influence on MPA-mediated GOx-PA binding; that is, no discernible difference was found in the enzyme binding to SnO_2 and to SnO_2 that had been exposed to MPA.

Assembly of the In-Line Filtration System and Determination of Glucose Consumption in Flow-Through Catalysis: GOx-PA loaded particles were charged into an inline filtration system by pipetting 0.2 mL of the particle suspension (in a 50 mM Tris-HCl buffer, pH 7.0) onto a nylon membrane (size of pores: 200 nm diameter) supported by a stainless steel mesh in an inline filter cartridge. The suspension was drained to form a powder bed, and covered with another nylon membrane on the top. An aqueous glucose solution was continuously circulated through the system at a flow rate of 10 mL min^{-1} from a continuously-stirred reservoir (50 mL) of a solution of glucose (20 mM) in sodium acetate buffer (100 mM, pH 5.5). To determine the rate of glucose decomposition, aliquots (0.2 mL) were periodically removed from the reservoir. The glucose concentration in the aliquots was determined by adding the Glucose (HK) Assay Reagent (200 µL, Sigma-Aldrich, St. Louis, MO) to the aliquots and then recording the absorbance at 340 nm. For a given specimen and flow-through time, repeated measurements of glucose consumption yielded values that agreed to within 5%.

Electron Microscopy: Scanning electron microscopy was conducted with a field emission gun instrument (Leo 1530 FEG SEM, Carl Zeiss SMT, Ltd., Thornwood, NY) that was equipped with an energy dispersive X-ray spectrometer (INCA EDS, Oxford Instruments). For transmission electron microscopy, the specimens were mixed with epoxy and then introduced into a copper tube (2.2 mm inner diameter). After curing of the epoxy, the tube was cut into disks (1 mm thick). The disks were then ground to a reduced thickness (100 µm), followed by dimpling and ion milling to perforation. Transmission electron microscopy was performed with a TECNAI F30 microscope (FEI, Hillsboro, Oregon USA) operated at 300 KV.

Surface Area and Pore Size Distribution Analysis: Nitrogen adsorption (BET) analyses were conducted using an Autosorb-1 Surface Area and Pore Size Analyzer (Quantachrome Instruments, Boynton Beach, FL). For evaluation of the specific mesopore and micropore volumes, 75 adsorption and 40 desorption points were recorded for a given specimen, and a NLDFT model for cylindrical pores was applied. Repeated measurements of the specific surface area, and the specific mesopore and micropore volumes, on a given specimen yielded values that agreed to within 5%.

XRD Analysis: Glancing angle X-ray diffraction (XRD) analyses were performed with an X-Pert Pro Alpha-1 diffractometer (PANalytical, B.V., Almelo, The Netherlands) at an incident angle of 1° using Cu Kα radiation with a Johannsen monochromator in the incident beam path and an X'Celerator linear detector.

XRF Analysis: X-ray fluorescence (XRF) measurements were conducted using a Mini-PAL 4 (PANalytical, B.V.) instrument, using Ag and Al X-ray sources. The PANalytical Omnian model was applied to determine the relative percentages of the elemental components.

FTIR Analysis: Samples were analyzed using an IR Prestige-21 spectrophotometer (Shimadzu Corp., Tokyo, Japan) equipped with a KBr beam splitter and DLaTGS detector that was utilized across the 400–3500 cm^{-1} range with a resolution of 4 or 8 cm^{-1}.

Zeta Potential Analysis: The zeta potential of the templates was determined in an aqueous solution of 100 mM Tris-HCl buffer (pH 7.0) using a Zetasizer Nano ZS instrument (Malvern Instruments, Ltd., Worcestershire, UK). The data were analyzed using the Smoluchowski Approximation[22] and General Mode Analysis in version 6.20 of the Malvern Zetasizer software.

Supporting Information

Supporting Information is available from the Wiley Online Library or from the author.

Acknowledgements

S.C.D. and V.C.S. contributed equally to this work. The work of S.C.D., V.C.S., G.B., N.K., K.H.S. was supported by the U.S. Department of Energy, Office of Basic Energy Sciences, Award No. DE-SC0002245. The work of J.D.B. and Y.C. was supported by the U.S. Air Force Office of Scientific Research, Award No. FA9550-09-1-0162. The work of Y.F. was supported by the U.S. Air Force Office of Scientific Research, Award No. FA9550-09-01-0669 (for surface functionalization) and No. FA9550-10-01-0555 (for displacive gold deposition). N.K. is grateful for support by the Research Corporation for Science Advancement and by the European Regional Development Fund (EFRE). The authors acknowledge the Georgia Tech FIB2 Center established under NSF funding.

Received: December 18, 2012
Revised: February 22, 2013
Published online: June 5, 2013

[1] a) R. C. Matos, J. J. Pedrotti, L. Angnes, *Anal. Chim. Acta* **2001**, *441*, 73; b) P. D'Orazio, *Clin. Chim. Acta* **2003**, *334*, 41; c) Y. Asanomi, H. Yamaguchi, M. Miyazaki, H. Maeda, *Molecules* **2011**, *16*, 6041; d) K. Faber, *Biotransformations in Organic Synthesis*, 5th ed., Springer-Verlag, Berlin **2004**; e) T. Larsson, A. Lindgren, T. Ruzgas, S.-E. Lindquist, L. Gorton, *J. Electroanal. Chem.* **2000**, *482*, 1; f) W. Zheng, H. M. Zhou, Y. F. Zheng, N. Wang, *Chem. Phys. Lett.* **2008**, *457*, 381; g) W. Feng, P. Ji, *Biotechnol. Adv.* **2011**, *29*, 889; h) B. Unnikrishnan, S. Palanisamy, S.-M. Chen, *Biosens. Bioelectron.* **2013**, *39*, 70.

[2] a) H. Takahashi, B. Li, T. Sasaki, C. Miyazaki, T. Kajino, S. Inagaki, *Chem. Mater.* **2000**, *12*, 3301; b) J. Aburto, M. Ayala, I. Bustos-Jaimes, C. Montiel, E. Terres, J. M. Dominguez, E. Torres, *Micropor. Mesopor. Mater.* **2005**, *83*, 193; c) J. Kim, H. Jia, P. Wang, *Biotechnol. Adv.* **2006**, *24*, 296.

[3] a) J. L. Blin, C. Gérardin, C. Carteret, L. Rodehüser, C. Selve, M. J. Stébé, *Chem. Mater.* **2005**, *17*, 1479; b) X. Zhang, R. F. Guan, D. Q. Wu, K. Y. Chan, *J. Mol. Catal. B Enzym.* **2005**, *33*, 43; c) H. H. P. Yiu, P. A. Wright, *J. Mater. Chem.* **2005**, *15*, 3690; d) E. Santalla, E. Serra, A. Mayoral, J. Losada, R. M. Blanco, I. Díaz, *Solid State Sci.* **2011**, *13*, 691.

[4] a) J. E. Bailey, Y, K. Cho, *Biotechnol. Bioeng.* **1983**, *25*, 1923; b) V. Vamvakaki, K. Tsagaraki, N. A. Chaniotakis, *Anal. Chem.* **2006**, *78*, 5538; c) D. C. Goldstein, P. Thordarson, J. R. Peterson, *Aust. J. Chem.* **2009**, *62*, 1320; d) H. Wen, V. Nallathambi, D. Chakraborty, S. Calabrese Barton, *Microchim. Acta* **2011**, *175*, 283; e) K. Min, J. Kim, K. Park, Y. J. Yoo, *J. Mol. Catal. B* **2012**, *83*, 87.

[5] a) A. L. Crumbliss, S. C. Perine, I. Stonehurner, K. R. Tubergen, I. Zhao, R. W. Henkens, I. P. O'Daly, *Biotechnol. Bioeng.* **1992**, *40*, 483; b) X. Wang, M. Falk, R. Ortiz, H. Matsumura, J. Bobacka, R. Ludwig, M. Bergelin, L. Gorton, S. Shleev, *Biosens. Bioelectron.* **2012**, *31*, 219.

[6] a) M. L. Mena, P. Yanez-Sedeno, J. M. Pingarron, *Anal. Biochem.* **2005**, *336*, 20; b) X. Luo, A. J. Killard, M. R. Smyth, *Electroanal.* **2006**, *18*, 1131; c) S. Wu, H. Ju, Y. Liu, *Adv. Funct. Mater.* **2007**, *17*, 585; d) Y. Bai, H. Yang, W. Yang, Y. Li, C. Sun, *Sens. Actuators, B* **2007**, *124*, 179; e) R. B. Rakhi, K. Sethupathi, S. Ramaprabhu, *J. Phys. Chem. B* **2009**, *113*, 3190.

[7] a) D. Lee, J. Lee, J. Kim, J. Kim, H. B. Na, B. Kim, C.-H. Shin, J. H. Kwak, A. Dohnalkova, J. W. Grate, T. Hyeon, H.-S. Kim, *Adv. Mater.* **2005**, *17*, 2828; b) M. Tortajada, D. Ramón, D. Beltrán, P. Amorós, *J. Mater. Chem.* **2005**, *15*, 3859; c) K. Nakanishi, N. Tanaka, *Acc. Chem. Res.* **2007**, *40*, 863; d) V. Flexer, N. Brun, R. Backov, N. Mano, *Energy Environ. Sci.* **2010**, *3*, 1302; e) Z. L. Hua, J. Zhou, J. L. Shi, *Chem. Commun.* **2011**, *47*, 10536; f) A. Sachse, A. Galarneau, F. Fajula, F. Di Renzo, P. Creux, B. Coq, *Micropor. Mesopor. Mater.* **2011**, *140*, 58; g) L. C. Cides da Silva, C. M. C. Infante, A. W. O. Lima, I. C. Cosentino, M. C. A. Fantini, F. R. P. Rocha, J. C. Masini, J. R. Matos, *J. Mol. Catal. B* **2011**, *70*, 149; h) B. Luangon, A. Siyasukh, P. Winayanuwattikun, W. Tanthapanichakoon, N. Tonanon, *J. Mol. Catal. B* **2012**, *75*, 80; i) A. H. Dessources, S. Hartmann, M. Baba, N. Huesing, J. M. Nedelec, *J. Mater. Chem.* **2012**, *22*, 2713; j) S. Lu, Z. An, J. He, B. Li, *J. Mater. Chem.* **2012**, *22*, 3882.

[8] a) F. E Round, R. M. Crawford, D. G. Mann, *The Diatoms: Biology and Morphology of the Genera*, Cambridge University Press, New York **1990**; b) D. G. Mann, S. J. M. Droop, *Hydrobiologia* **1996**, *336*, 19; c) R. Gordon, F. A. S. Sterrenburg, K. H. Sandhage, *J. Nanosci. Nanotechnol.* **2005**, *5*, 1; d) M. Hildebrand, *Chem. Rev.* **2008**, *108*, 4855; e) N. Kroger, N. Poulsen, *Ann. Rev. Gen.* **2008**, *42*, 83.

[9] a) K. H. Sandhage, M. B. Dickerson, P. M. Huseman, M. A. Caranna, J. D. Clifton, T. A. Bull, T. J. Heibel, W. R. Overton, M. E. A. Schoenwaelder, *Adv. Mater.* **2002**, *14*, 429; b) R. R. Unocic, F. M. Zalar, P. M. Sarosi, Y. Cai, K. H. Sandhage, *Chem. Comm.* **2004**, 795; c) Y. Cai, S. M. Allan, F. M. Zalar, K. H. Sandhage, *J. Am. Ceram. Soc.* **2005**, *88*, 2005; d) S. Shian, Y. Cai, M. R. Weatherspoon, S. M. Allan, K. H. Sandhage, *J. Am. Ceram. Soc.* **2006**, *89*, 694; e) S.-J. Lee, S. Shian, Ch.-H. Huang, K. H. Sandhage, *J. Am. Ceram. Soc.* **2007**, *90*, 1632; f) Z. Bao, M. R. Weatherspoon, Y. Cai, S. Shian, P. D. Graham, S. M. Allan, G. Ahmad, M. B. Dickerson, B. C. Church, Z. Kang, C. J. Summers, H. W. Abernathy, III, M. Liu, K. H. Sandhage, *Nature* **2007**, *446*, 172; g) Z. Bao, M.-K. Song, S. Davis, Y. Cai, M. Liu, K. H. Sandhage, *Energy Environ. Sci.* **2011**, *4*, 3980.

[10] a) N. L. Rosi, C. S. Thaxton, C. A. Mirkin, *Angew. Chem. Int. Ed.* **2004**, *43*, 5500; b) C. S. Gaddis, K. H. Sandhage, *J. Mater. Res.* **2004**, *19*, 2541; c) J. Zhao, C. S. Gaddis, Y. Cai, K. H. Sandhage, *J. Mater. Res.* **2005**, *20*, 282; d) D. Losic, G. Triani, P. J. Evans, A. Atancio, J. G. Mitchell, N. H. Voelcker, *Chem. Commun.* **2005**, 4905; e) S. M. Holmes, B. E. Graniel-Garcia, P. Foran, P. Hill, E. P. L. Roberts, B. H. Sakakini, J. M. Newton, *Chem. Commun.* **2006**, 2662; f) X. Cai, G. Zhu, W. Zhang, H. Zhao, C. Wang, S. Qiu, Y. Wei, *Eur. J. Inorg. Chem.* **2006**, 3641; g) M. R. Weatherspoon, M. B. Dickerson, G. Wang, Y. Cai, S. Shian, S. C. Jones, S. R. Marder, K. H. Sandhage, *Angew. Chem. Int. Ed.* **2007**, *46*, 5724; h) U. Kusari, Z. Bao, Y. Cai, G. Ahmad, K. H. Sandhage, L. G. Sneddon, *Chem. Commun.* **2007**, 1177; i) Y. Fang, Q. Wu, M. B. Dickerson, Y. Cai, S. Shian, D. Berrigan, N. Poulsen, N. Kroger, K. H. Sandhage, *Chem. Mater.* **2009**, *21*, 5704; k) Y. Fang, V. W. Chen, Y. Cai, J. D. Berrigan, S. R. Marder, J. W. Perry, K. H. Sandhage, *Adv. Funct. Mater.* **2012**, *22*, 2550; m) Y A. Jantschke, A.-K. Herrmann, V. Lesnyak, A. Eychmuller, E. Brunner, *Chem. Asian J.* **2012**, *7*, 85.

[11] a) M. W. Anderson, S. M. Holmes, N. Hanif, C. S. Cundy, *Angew. Chem. Int. Ed.* **2000**, *39*, 2707; b) Y. Wang, Y. Tang, A. Dong, X. Wang, N. Ren, Z. Gao, *J. Mater. Chem.* **2002**, *12*, 1812; c) Y. Cai, K. H. Sandhage, *Phys. Status Solidi (A)* **2005**, *202*, R105; d) M. R. Weatherspoon, S. M. Allan, E. Hunt, Y. Cai, K. H. Sandhage, *Chem. Commun.* **2005**, 651; e) K. H. Sandhage, R. L. Snyder, G. Ahmad, S. M. Allan, Y. Cai, M. B. Dickerson, C. S. Gaddis, M. S. Haluska, S. Shian, M. R. Weatherspoon, R. A. Rapp, R. R. Unocic, F. M. Zalar, Y. Zhang, M. Hildebrand, B. P. Palenik, *Int. J. Appl. Ceram. Technol.* **2005**, *2*, 317; f) M. R. Weatherspoon, M. S. Haluska, Y. Cai, J. S. King, C. J. Summers, R. L. Snyder, K. H. Sandhage, *J. Electrochem. Soc.* **2006**, *153*, H34; g) Y. Cai, M. B. Dickerson, M. S. Haluska, Z. Kang, C. J. Summers, K. H. Sandhage, *J. Am. Ceram. Soc.* **2007**, *90*, 1304; h) E. M. Ernst, B. C. Church, C. S. Gaddis, R. L. Snyder, K. H. Sandhage, *J. Mater. Res.* **2007**, *22*, 1121; i) K. H. Sandhage, **JOM 2010**, *62*, 32.

[12] a) J. R. Dyer, *Applications of Absorption Spectroscopy of Organic Compounds*, Prentice-Hall of India Private Limited, New Delhi, **1984**, Ch. 3; b) T. I. Hukka, J. Zhang, *J. Phys. Chem. B* **2000**, *104*, 7115; c) W. Shi, Y. Sahoo, M. T. Swihart, *Colloids Surf. A* **2004**, *246*, 109.

[13] a) Y. Matsumura, S. Hagiwara, H. Takahashi, *Carbon* **1976**, *14*, 163; b) Y. Otake, R. G. Jenkins, *Carbon* **1993**, *31*, 109; c) H. P. Boehm, *Carbon* **1994**, *32*, 759; d) N. Zhang, L. Wang, H. Liu, Q. Cai, *Surf. Interface Anal.* **2008**, *40*, 1190.
[14] a) G. Mattson, E. Conklin, S. Desai, G. Nielander, M. D. Savage, S. Morgensen, *Mol. Biol. Rep.* **1993**, *17*, 167; b) G. Wang, Y. Fang, P. Kim, A. Hayek, M. R. Weatherspoon, J. W. Perry, K. H. Sandhage, S. R. Marder, S. C. Jones, *Adv. Funct. Mater.* **2009**, *19*, 2768.
[15] a) Z. Bao, E. M. Ernst, S. Yoo, K. H. Sandhage, *Adv. Mater.* **2009**, *21*, 474; b) Y. Yu, J. Addai-Mensah, D. Losic, *Languir* **2010**, *26*, 14068.
[16] V. P. Menon, C. R. Martin, *Anal. Chem.* **1995**, *67*, 1920.
[17] a) Y. Sun, B. T. Mayers, Y. Xia, *Nano Lett.* **2002**, *5*, 481; b) Y. Sun, Y. Xia, *Science* **2002**, *298*, 2176.
[18] Powder Diffraction File, Card No. 01-071-4615 for Au, Card No. 01-071-4612 for Ag, Card No. 01-070-6153 for SnO_2 (International Center on Diffraction Data, Newtown Square, PA).
[19] a) W. Shi, Y. Sahoo, M. T. Swihart, *Colloids Surf. A* **2004**, *246*, 109; b) S.-F. Liu, X-H. Li, Y-C. Li, Y-F. Li, J-R. Li, L. Jiang, *Electrochim. Acta* **2005**, *51*, 427; c) G. A. Petkova, C. K. C. Záruba, P. Zvatora, V. Kral, *Nanoscale Res. Lett.* **2012**, *7*, 287.
[20] C. M. Wong, K. H. Wong, X. D. Chen, *Appl. Microbiol. Biotechnol.* **2008**, *78*, 927.
[21] N. R. Haase, S. Shian, K. H. Sandhage, N. Kröger, *Adv. Funct. Mater.* **2011**, *21*, 4243.
[22] M. von Smoluchowski, *Bull. Int. Acad. Sci. Cracovie* **1903**, *1*, 184.